Acetylcholine Receptor Organization in Membrane Domains in Muscle Cells

EVIDENCE FOR RAPSYN-INDEPENDENT AND RAPSYN-DEPENDENT MECHANISMS*

Joachim Piguet, Christoph Schreiter[1], Jean-Manuel Segura[2], Horst Vogel[3], and Ruud Hovius[4]

From the Laboratoire de Chimie Physique des Polymères et Membranes, Ecole Polytechnique Fédérale de Lausanne (EPFL), CH-1015 Lausanne, Switzerland

Nicotinic acetylcholine receptors (nAChR) in muscle fibers are densely packed in the postsynaptic region at the neuromuscular junction. Rapsyn plays a central role in directing and clustering nAChR during cellular differentiation and neuromuscular junction formation; however, it has not been demonstrated whether rapsyn is the only cause of receptor immobilization. Here, we used single-molecule tracking methods to investigate nAChR mobility in plasma membranes of myoblast cells during their differentiation to myotubes in the presence and absence of rapsyn. We found that in myoblasts the majority of nAChR were immobile and that ~20% of the receptors showed restricted diffusion in small domains of ~50 nm. In myoblasts devoid of rapsyn, the fraction of mobile nAChR was considerably increased, accompanied by a 3-fold decrease in the immobile population of nAChR with respect to rapsyn-expressing cells. Half of the mobile receptors were confined to domains of ~120 nm. Measurements performed in heterologously transfected HEK cells confirmed the direct immobilization of nAChR by rapsyn. However, irrespective of the presence of rapsyn, about one-third of nAChR were confined in 300-nm domains. Our results show (i) that rapsyn efficiently immobilizes nAChR independently of other postsynaptic scaffold components; (ii) nAChR is constrained in confined membrane domains independently of rapsyn; and (iii) in the presence of rapsyn, the size of these domains is strongly reduced.

Neuromuscular junctions (NMJ)[5] are long-lasting synapses mediating signal transmission between neurons and skeletal muscle cells (1). The postsynaptic membrane of the NMJ comprises a high density ($\sim$10,000 copies/μm^2) of nicotinic acetylcholine receptors (nAChR) bound noncovalently to a specific scaffolding protein network through a 1:1 interaction with rapsyn (2–5). The high density and the precise location of nAChR in the muscle fiber directly beneath a nerve terminal are essential for fast and robust signal transmission.

The presence of nAChR at the NMJ during development depends on agrin, a heparan sulfate proteoglycan secreted by the presynaptic motor neuron (6), and rapsyn (7). Agrin activates the muscle-specific tyrosine kinase MuSK through binding to its co-receptor LPR4 (8, 9), which leads to phosphorylation of the β-subunit of nAChR (3) and in turn to local receptor clustering at the nerve terminus (10). Rapsyn binding to MuSK is required for this phosphorylation step (11, 12). Wnt was recently found to play a role in nAChR cluster formation during muscle development (13). Agrin and Wnt regulate the distribution of nAChR in the postsynaptic membrane by increasing receptor density in the NMJ and decreasing receptor density outside the NMJ (14). During these processes, rapsyn directs nAChR into contact with other NMJ proteins without altering channel function (15). Rapsyn is also found at high concentrations together with nAChR in membranes of the electric organ of *Torpedo* (16) and in the developing neuromuscular synapse of *Xenopus* (7).

The myristoylated N terminus of rapsyn targets the protein to the plasma membrane, where it participates in a number of important additional molecular interactions (17). (i) Rapsyn self-associates through its seven tetratricopeptide repeats (18, 19). (ii) It binds to the cytoskeleton via an ACF7-containing network (20). (iii) It also binds to other molecules of the NMJ, such as calpain (21), β-catenin (22), and α-actinin (23).

Failure in nAChR anchoring at the NMJ endplate causes defects in neuromuscular synaptic transmission, leading to severe myopathies (24). Understanding the mechanism of nAChR anchoring is therefore of importance for finding ways to treat muscular diseases. In general, membrane proteins reveal complex mobility patterns in living cells, including unrestricted (Brownian) diffusion, restricted diffusion within micrometer- to nanometer-sized membrane domains, or even totally immobile receptors (25), the relative proportions of which can change substantially during biogenesis of a cell.

Here, we investigated the mobility patterns and lateral diffusion of nAChR and its interacting protein rapsyn in muscle cells during different stages of differentiation to elucidate how rapsyn modulates nAChR. To address these questions, we use single-molecule imaging to follow the spatiotemporal distribution of nAChR in different cell lines and thus resolve mo-

[1] Present address: 24IP Law Group, D-80331 München, Germany.
[2] Present address: Inst. of Life Technologies, University of Applied Sciences, Western Switzerland Valais, Rte. de Rawyl 64, CH-1950 Sion, Switzerland.
[3] To whom correspondence may be addressed. Tel.: 41-21-693-3155; Fax: 41-21-693-6190; E-mail: horst.vogel@epfl.ch.
[4] To whom correspondence may be addressed. Tel.: 41-21-693-3134; Fax: 41-21-693-6190; E-mail: ruud.hovius@epfl.ch.

[5] The abbreviations used are: NMJ, neuromuscular junction(s); nAChR, nicotinic acetylcholine receptor(s); α-CnTx, α-conotoxin GI; α-BgTx, α-bungarotoxin; QD, quantum dot(s); MSD, mean square displacement; MSS, moment scaling spectrum.

bility patterns, which would be undistinguishable when using ensemble measurements.

Optical imaging requires labeling of the proteins of interest with fluorescent probes. Here, we approached this problem by labeling native nAChR with small fluorescent toxins, either reversibly with fluorescent α-conotoxin (2.7 kDa) (26) or quasi-irreversibly with fluorescent α-bungarotoxin. This approach offers a substantial advantage working with native receptors instead of genetically engineered receptors fused either with fluorescent proteins (27) or with tags for post-translational labeling (28).

EXPERIMENTAL PROCEDURES

Cell Culture and Transfection—Myogenic cell lines C2C12 (a C2 myoblast) and R11 (a rapsyn$^{-/-}$ myoblast) were grown and differentiated to myotubes. C2C12 cells (obtained from U. Rüegg, University of Geneva) were grown in DMEM/F-12 (Invitrogen) supplemented with 10% FBS (Sigma), 100 units/ml penicillin, and 100 μg/ml streptomycin. R11 myoblasts (obtained from C. Fuhrer) (15) were grown in DMEM (Invitrogen) supplemented with 10% FBS, 100 units/ml penicillin, 100 μg/ml streptomycin, and 4 units/ml γ-interferon (Sigma). Cells were maintained at 34 °C in a humidified 5% CO_2 atmosphere. For imaging, cells were seeded on 0.17-mm thick glass coverslips. Differentiation to myotubes was induced at 80% confluency by changing the medium to DMEM supplemented with 5% horse serum (Sigma) and growing at 37 °C in a humidified 5% CO_2 atmosphere.

HEK 293T cells (American Type Culture Collection) were grown in DMEM/F-12 supplemented with 10% FBS at 37 °C in a humidified 5% CO_2 atmosphere. Cells were plated on 25-mm diameter glass coverslips in a 30-mm diameter well and transfected 24 h later using Effectene (Qiagen) with cDNAs of nAChR subunits (60 ng of α-subunit, 30 ng of β-subunit, 30 ng of γ-subunit, and 30 ng of δ-subunit) and 30 ng of either enhanced GFP (Clontech) or rapsyn-GFP (generous gift from J. Cohen) (18). Compared with enhanced GFP, this GFP has similar spectral properties but with two mutated residues (L65F and L231H). Single molecules were imaged on cells 24–48 h after transfection in colorless DMEM or Hanks' balanced salt solution (both from Invitrogen) without antibiotics and serum.

Receptor Labeling—nAChR in living cells were visualized using either α-conotoxin GI (α-CnTx) conjugated with organic fluorophores or α-bungarotoxin (α-BgTx) coupled to fluorescent semiconductor quantum dots (QD). Labeling of nAChR with α-CnTx conjugated with either Cy5 (GE Healthcare) or ATTO 647N (ATTO-TEC) was performed using the repetitive reversible labeling method described in detail previously (26, 29).

Briefly, cells were perfused using a VC-77SP fast step perfusion system (Warner Instruments Corp.) for 10 s with 30 nM fluorescent α-CnTx labeling ~1–5% of the nAChR expressed on the cell surface, followed by 20 s with Hanks' balanced salt solution, after which fluorescent image series were acquired. This sequence was repeated at will, enabling us to measure diffusion of a large number of individual receptors on one single cell repetitively despite fast bleaching of the organic dyes.

Alternatively, streptavidin-coated fluorescent QD (kindly provided by M. Bäumle, Fluka) were incubated with α-BgTx-biotin (Sigma) at a ratio of one toxin molecule/two QD. Myoblasts were labeled with 500 pM α-BgTx-NP conjugates in DMEM for 60 min at 37 °C. Prior to microscopy measurements, the cells were rinsed three times in colorless DMEM to remove unbound probes.

Single-molecule Microscopy—Glass coverslips were mounted on a modified epiluminescence wide-field microscope (Axiovert 200, Zeiss). Fluorescently labeled α-CnTx was excited with circularly polarized light at 632.8 nm (HeNe laser, Coherent Inc.) that was directed by a dichroic mirror (Q645LP, Chroma Corp.) into a water immersion objective (C-Apochromat 63×/W Korr, 1.2 numerical aperture, Zeiss) to illuminate a 22-μm diameter region of the sample. Fluorescence emission was collected by the same objective, passed through a filter (HQ710/100, Chroma Corp.), and imaged on an intensified CCD camera (Ixon 887BV, Andor). To minimize photobleaching of organic dyes, cells were illuminated for 50 ms with excitation intensities of 0.5 kilowatts/cm^2 only during image acquisition using a shutter (LS3T2, Vincent Associates). Single-molecule images were recorded at a frequency of 4–20 Hz. Dissociation of α-CnTx from nAChR was much slower than photobleaching as described in detail previously (26).

α-BgTx-QD conjugates were excited at 488 nm (Ar$^+$ laser, Innova Sabre). A circularly polarized laser beam was directed by a Q495LP dichroic mirror (Chroma Corp.) into the objective. Fluorescence emission was collected by the same objective and imaged after passing through a HQ595/50 dichroic filter (Chroma Corp.). Single-molecule images were recorded at a frequency of 20 Hz, illuminating the cells for 48.3 ms with excitation intensities of 0.1 kilowatts/cm^2. Single-molecule trajectories were measured at the apical membrane of the cells to avoid unwanted effects of cell adhesion and fluorophore accumulation on the glass surface.

Data Evaluation—Images were analyzed using a home-written IGOR Pro program (WaveMetrics). Each image was first filtered to remove long-range structures such as the laser intensity profile and autofluorescence of the cells. Next, fluorescent spots were identified on the filtered image. Fluorescent spots were then fitted with a two-dimensional Gaussian function on the original unfiltered image. Fitted fluorescent spots corresponding to single molecules were evaluated for intensity and tracked over a series of images to evaluate single-molecule trajectories. Characteristic one-step photobleaching or blinking events were taken as a criterion for selecting a single-molecule trace. Finally, square displacements (r^2) were evaluated for every time interval of a single trajectory.

Single-molecule traces were treated using two different strategies. Data sets of short traces resulting from experiments with organic dyes were evaluated according to Schütz *et al.* (30). Briefly, the normalized cumulative probability density function ($P(r^2,t_{lag})$) of r^2 was evaluated for each time lag (t_{lag}). This $P(r^2,t_{lag})$ was then fitted using Equation 1 or 2,

yielding one or two average square displacements (r_0^2), respectively.

$$P(r^2, t_{\text{lag}}) = 1 - \exp\left(\frac{r^2}{r_0^2(t_{\text{lag}})}\right) \quad \text{(Eq. 1)}$$

$$P(r^2, t_{\text{lag}}) = 1 - \left(\alpha \cdot \exp\left(\frac{r^2}{r_1^2(t_{\text{lag}})}\right) + (1 - \alpha) \cdot \exp\left(\frac{r^2}{r_2^2(t_{\text{lag}})}\right)\right) \quad \text{(Eq. 2)}$$

In Equation 2, α is the fraction of the two average square displacements (r_1^2 and r_2^2) for each time lag. The diffusion coefficient (D) for each population is then deduced using a standard mean square displacement (MSD) *versus* t_{lag} fit, according to Equations 3 and 4. Whenever possible, in longer trajectories, the apparent confinement length (L_c) and initial diffusion coefficient (D_0) were also evaluated. D_0 was determined from a linear fit of data points 2–4 of the plot of MSD *versus* t_{lag} (Equation 3). This value was used to separate mobile and immobile receptors by setting a noise-dependent threshold. MSD plots of individual receptors were fitted using an approximation of a single molecule in a square, yielding an apparent D_0 and L_c corresponding to the diagonal of a rectangle enclosing the diffusing object (Equation 4) (30–32). The noise term added in each equation is due to the noise of the CCD image and the movement of the particle during the acquisition time.

$$\text{MSD}(t_{\text{lag}}) = 4 \cdot D_0 \cdot t_{\text{lag}} + \text{noise} \quad \text{(Eq. 3)}$$

$$\text{MSD}(t_{\text{lag}}) = \frac{L_c^2}{3}\left(1 - \exp\left(\frac{-12 \cdot D_0 \cdot t_{\text{lag}}}{L_c^2}\right)\right) + \text{noise} \quad \text{(Eq. 4)}$$

As the diffusion of a particle is a self-similar process, long single-molecule trajectories can be treated using the moment scaling spectrum (MSS). This method gives more accurate information about the type of motion and, as it involves only linear fits, avoids errors arising from complex multiparameter fits (33, 34). The MSS slope is a single parameter that allows us to distinguish between anomalous, directed, and confined diffusion: a slope of 0.5 defines Brownian motion; values <0.5 and >0 are characteristic of confined motion; values equal to zero indicate immobility; and values >0.5 describe directed diffusion (33). Each MMS slope was computed using a sliding window of 60 frames.

RESULTS

Mobility of nAChR in C2C12 Mouse Muscle Cells during Differentiation—C2C12 muscle cells differentiate into functional myotubes within 5 days after the addition of 5% horse serum to the cell culture medium. Diffusion of nAChR in the cell plasma membrane was measured by single-receptor tracking before and 2, 3, 5, 8, and 11 days after induction of differentiation. During this time period, significant changes were observed in the membrane distribution of nAChR, visualized by receptor-bound fluorescent toxins (Fig. 1). Before differentiation, nAChR was homogeneously distributed in the
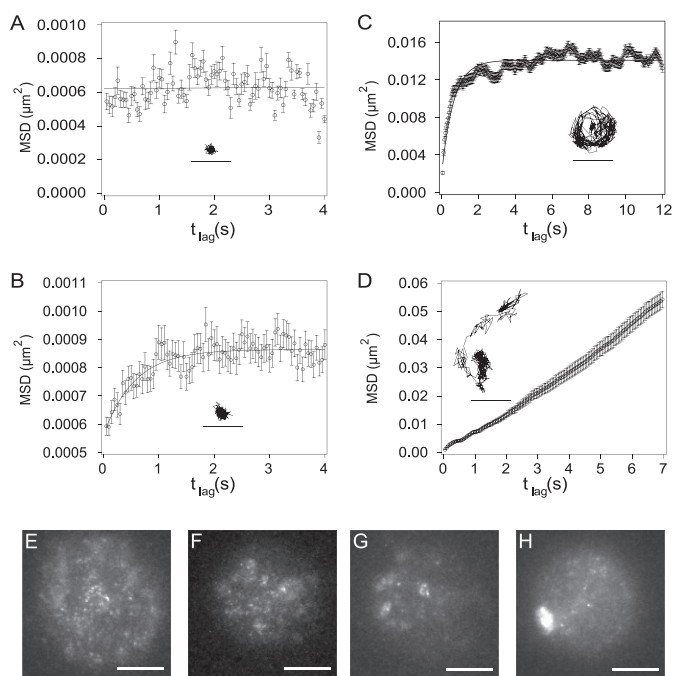

FIGURE 1. **Typical MSD *versus* t_{lag} plots and fluorescence micrographs of nAChR in the apical membrane of C2C12 myotubes.** Three characteristic modes of motion were observed for nAChR labeled with α-BgTx-QD in C2C12 muscle cells. Representative single-molecule trajectories (*scale bars* = 100 nm) are depicted as *insets* in the corresponding MSD *versus* t_{lag} plots (*scale bars* = 100 nm). *A*, an immobile receptor. The positive *y intercept* is due to experimental noise. In this case, the position accuracy of measurement is 12 ± 2 nm, which is typical for quantum dots on living cells with our experimental setup. *B*, a receptor confined in a small domain with a characteristic length of $L_c = 30 \pm 1$ nm and a diffusion coefficient of $D_0 = (1.3 \pm 0.2) \times 10^{-4} \ \mu\text{m}^2/\text{s}$. *C*, a receptor confined in a domain with a characteristic length of $L_c = 189 \pm 1$ nm and a diffusion coefficient of $D_0 = (4.6 \pm 0.2) \times 10^{-3} \ \mu\text{m}^2/\text{s}$. *D*, a mobile receptor with a diffusion coefficient of $D_0 = (1.48 \pm 0.03) \times 10^{-3} \ \mu\text{m}^2/\text{s}$. The receptor exhibited a small positive deviation from the linearity due to sample movement and potentially directed motion of the receptor. The speed of this supplementary motion was 15 nm/s. Images are of nAChR labeled with α-CnTx-Cy5 taken by a wide-field microscope after five frames corresponding to a total illumination time of 250 ms. The illuminated area is limited to a single cell. *E*, myoblast cells before differentiation show nAChR homogeneously distributed. *F*, 2 days after culture medium exchange, receptor distribution is still homogeneous. *G*, 3 days after culture medium exchange, denser and larger regions are visible. *H*, in a multinucleated cell 8 days after culture medium exchange, dense clusters of receptors are visible. *Scale bars* = 10 μm.

membrane (Fig. 1*E*). The same homogeneous distribution was observed still after 2 days (Fig. 1*F*). Mononucleated cells began to align after 3 days, and dense receptor clusters became visible at the cell membrane even in the absence of presynaptically secreted agrin (Fig. 1*G*). After 5 days, when most of the cells were fused to multinucleated cells and began to form myotubes, dense clusters of nAChR appeared (Fig. 1*H*).

Three different populations of nAChR were observed in the plasma membrane of muscle cells: immobile, confined, and freely diffusing receptors. Fig. 2 depicts representative plots of MSD *versus* t_{lag} of single-receptor trajectories. For Brownian diffusion, MSD is linearly dependent on time; deviations from linearity indicate non-ideal diffusion (35). Here, we characterized the trajectories of individual nAChR according to two parameters: (i) the initial D_0 of the receptor and (ii) the L_c of its confinement region. The value of D_0 was used to distinguish between mobile and immobile receptors, and that of L_c
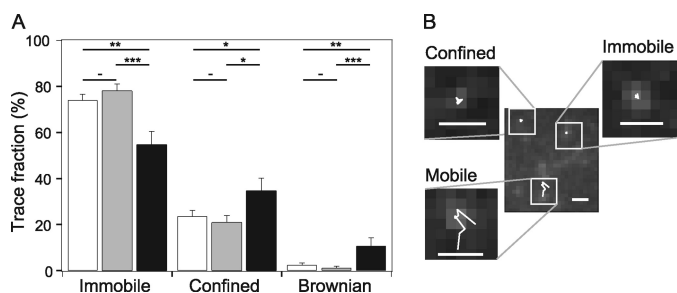
FIGURE 2. **Evolution of the fraction of immobile, confined, and freely diffusing receptors in differentiating C2C12 muscle cells.** *A*, nAChR was labeled with α-CnTx-Cy5, and images were acquired at 4 Hz. *White bars* correspond to measurements on C2C12 myoblasts before induction of differentiation ($n = 292$). *Gray bars* show receptor mobility during differentiation (days 2, 3, and 5) ($n = 182$). *Black bars* correspond to receptors in multinucleated muscle fibers (days 8 and 12) ($n = 75$). *, $p < 0.05$ (*t* test); **, $p < 0.01$; ***, $p < 0.001$ *B*, trajectories corresponding to the three characteristic modes of motion. *Scale bars* = 1 μm.

FIGURE 3. **Mobility of nAChR in muscle cells obtained by MSS data treatment.** *A* and *B*, MSS slope *versus* D_0 for rapsyn$^{+/+}$ (C2C12) cells and rapsyn$^{-/-}$ (R11) cells, respectively. Each of the points was computed from a receptor trajectory longer than 100 frames. For Brownian diffusion, the MSS slope is equal to 0.5. Values <0.5 denote a confined receptor, a value of 0 corresponds to an immobile molecule, values >0.5 show superdiffusion, and a value of 1 corresponds to directed motion. *Top* and *side panels* represent histograms of D_0 and MSS slope, respectively. *C*, fractions of receptors in the three different categories in R11 (*white bars*) and C2C12 (*black bars*) myoblasts. **, $p < 0.01$; ***, $p < 0.001$.

was used to discriminate confined ($L_c < 280$ nm) from freely diffusing receptors.

Individual nAChR were visualized after binding of α-CnTx covalently labeled with the fluorescent probe Cy5, yielding single-receptor trajectories of up to 40 frames acquired at 4 Hz. Single-receptor trajectories were measured using cells at three different states of development: before induction (undifferentiated myoblasts), during differentiation (days 2, 3, and 5), and after differentiation (multinucleated myotubes at days 8 and 11) (Fig. 2). Before differentiation, only 2% of the receptors showed free Brownian diffusion, 24% diffused in confined regions, and 74% were immobile. During differentiation and cell fusion, the immobile receptor fraction increased slightly without a significant effect on the two other types of receptor mobility. However, in differentiated multinucleated cells, the proportion of immobile receptors decreased strongly, with a concomitant increase in the fraction of confined diffusing receptors from 20 to 34% and of freely diffusing receptors up to 10%. At all times, the majority (>60%) of the confined receptors were located in domains with $L_c < 100$ nm.

Diffusion of nAChR in Muscle Cells Devoid of Rapsyn—To investigate the direct effect of rapsyn on receptor mobility, trajectories of individual nAChR were measured on R11 rapsyn$^{-/-}$ mouse muscle cells, which are devoid of rapsyn (both alleles are inactivated). Because R11 muscle cells are difficult to differentiate into multinucleated myotubes, comparative experiments were carried on myoblasts.

Single-receptor trajectories of superior quality were obtained using toxins labeled with fluorescent probes of increased photostability (α-BgTx-NP and α-CnTx-ATTO 647N), yielding extremely long trajectories of up to 5 min (6000 frames at 20 Hz). For most experiments, however, we measured only up to 300 frames to reduce phototoxicity. The average lengths of the traces for C2C12 and R11 cells were 254 and 159 frames, respectively, due to trace interruption by blinking and bleaching. The yet substantially improved quality of the MSD *versus* t_{lag} plots allowed us to determine particular D_0 and L_c values with considerably increased accuracy. Moreover, the long traces allowed us to use the MSS data evaluation method (33) to unequivocally classify the type of mobility for single trajectories (see "Experimental Procedures"). Fig. 3
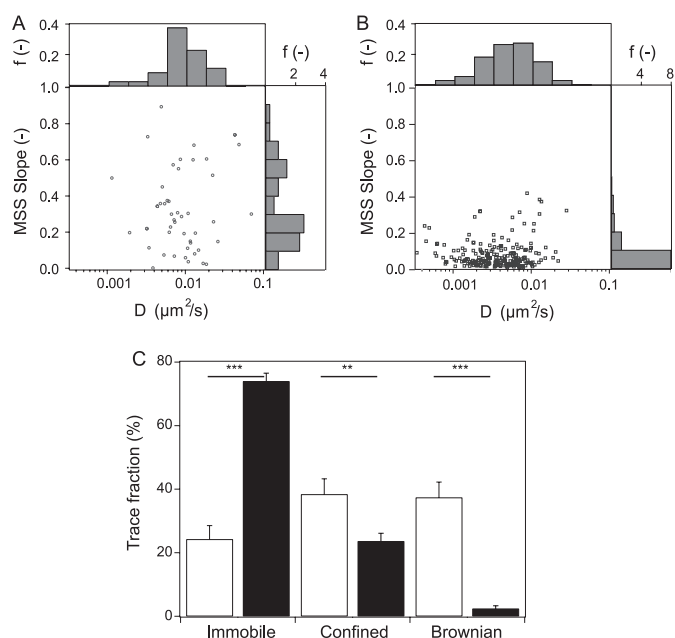
shows the resulting graphs of MSS slope *versus* D_0. There was a shift from immobile and confined receptors in the presence of rapsyn (0 < MSS slope < 0.4) to confined and freely mobile receptors in the absence of rapsyn (0.1 < MSS slope < 0.8). The median size of the observed confinement regions increased from 46 nm for C2C12 cells to 117 nm for R11 cells. Moreover, in the absence of rapsyn, the mobility of nAChR strongly increased as determined by D_0.

Despite the considerably long duration of the trajectories of up to 100 s, not a single case was observed in which an initially immobile or confined molecule switched to Brownian diffusion. However, some of the apparently freely diffusing receptors exhibited transient clustering. Fig. 4 shows one of the initially freely diffusing receptors being transiently trapped in domains, featuring transitions between free and confined motion and immobility.

Heterologous Expression of nAChR and Rapsyn—In muscle cells, many different proteins participate in scaffolding nAChR within the NMJ. To investigate the interaction between nAChR and rapsyn in the cell plasma membrane in the absence of other components of the NMJ, we expressed the proteins heterologously in HEK 293T cells. This cell line has been used as a neutral background to study the interaction between rapsyn and nAChR (36, 37), and no mRNA encoding rapsyn was detected (38). The mobility of nAChR was investigated under two different conditions: cells were transfected with cDNA of nAChR subunits together with either rapsyn-GFP or, as a control, cytosolic enhanced GFP. As before (Fig.
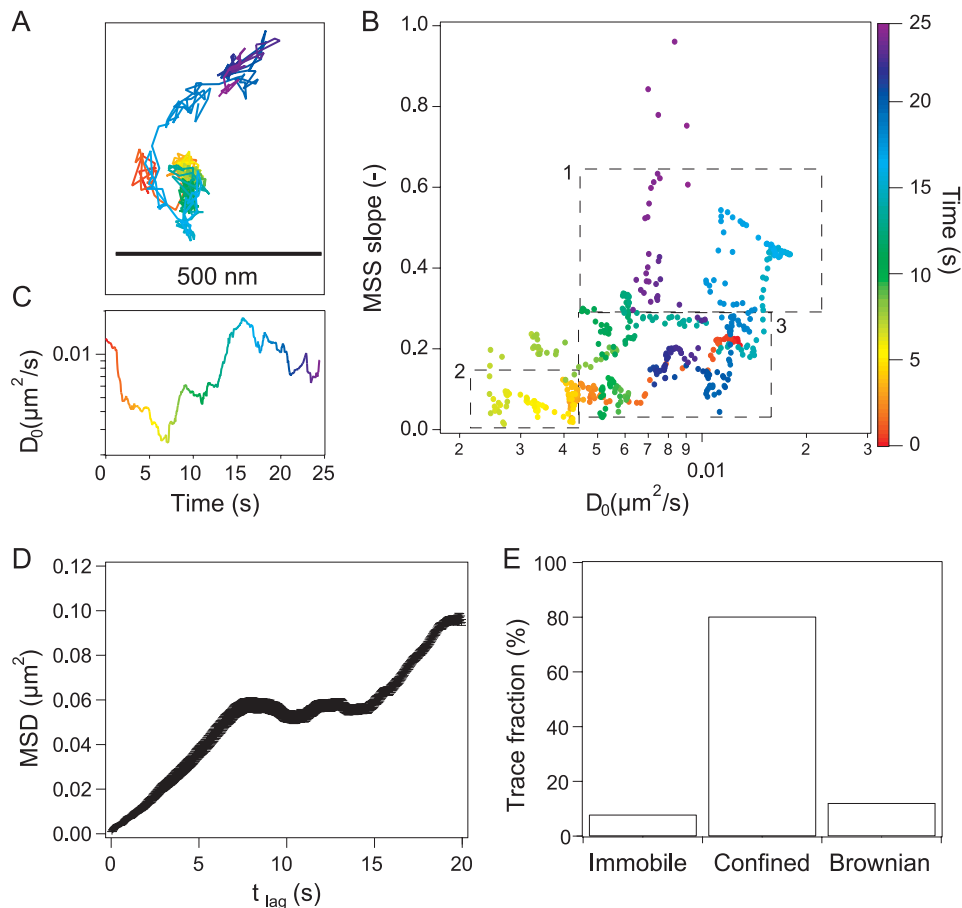
FIGURE 4. **Different representations and evaluations of the mobility of a single nAChR in the cell membrane.** This trajectory is of one of the only two nAChR exhibiting changes in diffusion modes during the measurement. Receptors in R11 rapsyn$^{-/-}$ muscle cells labeled with α-BgTx-QD and imaged at 20 Hz showed transient recruitment in membrane domains. *A*, trajectory of a single receptor. The color code indicates the time scale. *B*, MSS slope *versus* D_0, indicating different modes of diffusion of a single receptor. *Region 1* corresponds to freely diffusing receptor in the plasma membrane. *Region 2* corresponds to confined diffusion. *Region 3* corresponds to an immobilized receptor. At $t = 0$, the receptor is diffusing in a confined domain. Between $t = 2$ and 10 s, it is immobile and then it is alternating between confined and free Brownian motion. *C*, initial diffusion coefficient of each segment of the trajectory. This representation also shows transient trapping between 5 and 8 s. The color code as in *B*. *D*, MSD *versus* t_{lag} of this particular trajectory. The multiple diffusion modes of the particle are not visible in this representation. *E*, histogram representing the three modes of mobility. The distribution is in good agreement with the values obtained by the MSS data evaluation in *A*.
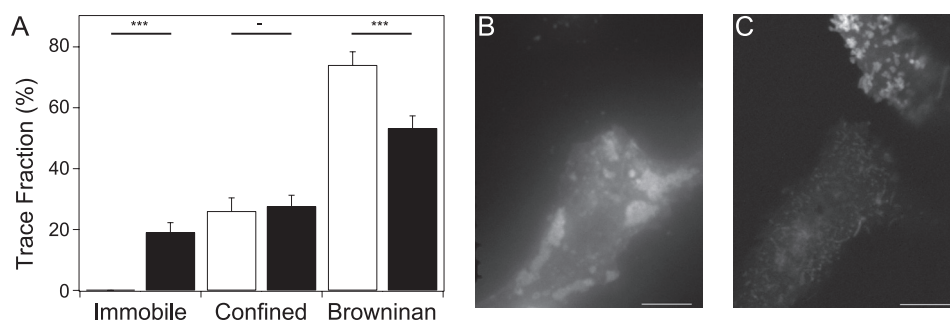

FIGURE 5. **Diffusion of nAChR in HEK 293T cells and distribution of fluorescent rapsyn in myoblasts and HEK cells.** *A*, fractions of immobile, confined, and freely diffusing nAChR in HEK 293T cells. *White bars* correspond to cells cotransfected with nAChR and enhanced GFP ($n = 108$). *Black bars* correspond to cells cotransfected with nAChR and rapsyn-GFP ($n = 163$). ***, $p < 0.001$. *B*, wide-field laser excitation of C2C12 myoblasts revealed large bright regions ($>1 \, \mu$m) corresponding to a high density of rapsyn-GFP. *C*, confocal fluorescence micrograph of HEK cells transiently expressing rapsyn-GFP, acquired with a Zeiss LSM 510 confocal microscope. The size of the bright domains is much smaller in the heterologous expression system than in the C2C12 myoblasts in *B*. *Scale bars* = 10 μm.

1), receptor mobility was classified into three categories according to the same criteria.

Upon expression of only nAChR in HEK 293T cells, we could not observe immobile receptors (Fig. 5). Mobile receptors were distinguished as those featuring Brownian or confined diffusion according to a cumulative distribution analysis

(30, 31). Freely diffusing ($55 \pm 2\%$) nAChR had a D_0 of $0.043 \pm 0.002 \, \mu$m^2/s; those showing confined diffusion were characterized by an initial D_0 of $0.016 \pm 0.005 \, \mu$m^2/s and a domain size of $L_c = 320 \pm 20$ nm.

Cotransfection of rapsyn-GFP and nAChR plasmids at a 1:1 molar ratio in HEK cells led to the formation of dense rapsyn

clusters at the cell membrane (Fig. 5C). Very strikingly, we observed a large population of immobile receptors (19%) with $D_0 < 0.005$ μm^2/s, a decreased population of freely diffusing receptors (53%), and a virtually unchanged fraction of receptors with confined diffusion (28%) with slightly increased L_c from 322 ± 21 to 377 ± 33 nm ($p < 0.001$) compared with the absence of GFP-rapsyn. The low proportion of labeled nAChR used for each image series did neither allow us to detect clusters of receptors nor to identify regions on the cell membrane of restricted nAChR diffusion.

DISCUSSION

Visualizing nAChR with Fluorescent Toxins—For imaging individual receptors on the cell surface, we developed two complementary staining procedures. (i) Using fluorescent α-CnTx, we could stain nAChR on the surface of myotubes both inside receptor clusters, *i.e.* in regions of high receptor density, and in membrane areas featuring low receptor density. The binding of fluorescent α-CnTx could be reversed, allowing sequential restaining (26). This yielded a large number of trajectories of single receptors, sampling many different receptors on the same cell, and thus improved substantially the reliability of determining the mobility of the receptors. (ii) Staining nAChR with virtually irreversibly bound α-BgTx-NP conjugates made it possible to acquire very long traces, revealing changes in the diffusion modes of nAChR.

Mobility of nAChR during Myotube Formation—Because C2C12 mouse myoblasts form postsynaptic-like structures after differentiation (39), we selected them as a model system to study receptor mobility in synapses. In undifferentiated C2C12 cells, no nAChR clusters were resolved, although ~70% of the receptors were immobile. Clusters of nAChR and rapsyn did appear only after 2 days of incubation in the differentiating culture medium, still before fusion of myoblasts to myotubes. The mobility of the receptors did not change until the cells became multinucleated, whereby the fraction of mobile receptors increased. This might be explained by the observation that during differentiation, although the rapsyn level remains constant, the expression of nAChR subunits increases, *i.e.* the rapsyn/nAChR ratio decreases (40). On the other hand, an increasing rapsyn *versus* nAChR concentration is known to slow down receptor turnover (41), which corroborates our finding that the nAChR mobility is lower in undifferentiated than in differentiated C2C12 cells. Our results suggest that individual nAChR are released from receptor-dense regions to move freely in the surrounding membrane bulk phase. Such a release could be important either for receptor recycling or for serving as a reservoir of receptors, outside the synapses.

The rate of change in nAChR mobility was quantified by calculating k_{change} = (number of changes)/(total measurement time). The rather short (few seconds) single-molecule trajectories obtained using α-CnTx labeled with organic fluorophores did not feature any change in receptor mobility within any of the evaluated 292 traces ($k_{change} < 2 \times 10^{-3}$ s^{-1}), implying that the receptors remain in a particular state. Long trajectories (tens of seconds) obtained with the photostable α-BgTx-NP conjugates showed a similar behavior. The low switching rate ($k_{change} < 3 \times 10^{-4}$ s^{-1}) could contribute to the stability of the NMJ.

From heterologously expressed nAChR in HEK cells devoid of rapsyn, only a few receptors (<1%) were immobile, whereas heterologously expressed rapsyn in HEK cells resulted in the appearance of a large fraction of immobilized nAChR (Fig. 5). These results confirmed that rapsyn alone can immobilize nAChR and induce small but significant increases in L_c.

In contrast, muscle cells feature a very large fraction of immobile receptors. Throughout differentiation, a substantial fraction of receptor diffused in confined regions (Fig. 2A). Thus, confinement of nAChR is not directly related to an increased expression of muscle-specific proteins associated with myotube formation and could be due to direct interactions of the receptor with the plasma membrane (42).

Immobile or strongly confined receptors were also found outside of nAChR clusters in C2C12 muscle cells. This observation suggests that not all complexes between rapsyn and nAChR are recruited in clusters in neuronal myotubes.

Clustering of nAChR—Whereas rapsyn forms dense domains at the cell membrane of myoblasts (Fig. 5), nAChR does not. However, nAChR is known to cluster in differentiated muscle cells. There are two possible explanations for these observations in myoblasts. (i) Receptors are present at such a low concentration that they are homogeneously distributed over the entire rapsyn-covered membrane domains. (ii) Apparently, the signals inducing clustering in differentiated cells are not present in myoblasts. The absence of nAChR clustering in HEK cells can be explained by its low expression upon transient transfection (<1000 copies/cell) (26).

Recruitment of nAChR in Membrane Domains—We have observed receptors diffusing in confined domains in both rapsyn$^{+/+}$ and rapsyn$^{-/-}$ myoblasts, indicating rapsyn-independent recruitment of nAChR in muscle cells with smaller L_c if rapsyn was present. Elsewhere, 50-nm membrane domains of nAChR have been observed by stimulated emission depletion microscopy in chemically fixed CHO cells (43). In the presence of a sufficient amount of rapsyn, nearly all formerly diffusing receptors were finally immobilized (Fig. 3).

The existence of very stable, receptor-rich domains in the plasma membrane might be due to endocytosis. nAChR colocalizes with caveolin-3, a major functional component of caveolae involved in agrin-induced clustering of nAChR (44–46). The values for L_c found here are comparable with the dimensions of 25–100 nm reported previously for caveolae (45). The small number of immobile receptors observed in R11 cells suggests the existence of a less efficient, rapsyn-independent mechanism of receptor immobilization. The long time of >15 s that the receptors remained immobilized (>300 frames) in our study is not fully comparable with transient receptor recruitment occurring in 50-nm membrane domains within the range of 0.5 s reported by Suzuki *et al.* (47). Specific, long lasting interactions with cytoskeleton components could explain our findings.

Transient Recruitment of nAChR—The very rare, transient recruitment events of nAChR, shown in Fig. 4, could be due to hindered diffusion in the cell plasma membrane (25), tran-

sient interactions with other components (48), or recruitment in short-living membrane domains (49). nAChR is claimed to partition into cholesterol-rich membrane domains after agrin activation (50). The transient immobilization events observed here might stem from short-living membrane domains.

Conclusion—Our single-receptor tracking experiments yielded a complex mobility pattern of muscle-type nAChR in the plasma membrane of different cell types: the presence of rapsyn increases the number of immobilized receptors and changes the size of the confinement for both the nAChR at natural abundance in muscle cells and the heterologously expressed nAChR in HEK cells. In muscle cells devoid of rapsyn, a fraction of nAChR remains immobilized and confined by an unknown mechanism. Single-receptor imaging also revealed the existence of small membrane regions comprising confined nAChR that are not related to large receptor clusters associated with rapsyn: the small confinement regions may serve as a complementary regulatory means for receptor store and release.

REFERENCES

1. Sanes, J. R., and Lichtman, J. W. (1999) *Annu. Rev. Neurosci.* **22,** 389–442
2. Bromann, P. A., Zhou, H., and Sanes, J. R. (2004) *Neuroscience* **125,** 417–426
3. Lee, Y., Rudell, J., and Ferns, M. (2009) *Neuroscience* **163,** 222–232
4. Frail, D. E., McLaughlin, L. L., Mudd, J., and Merlie, J. P. (1988) *J. Biol. Chem.* **263,** 15602–15607
5. Bruneau, E., and Akaaboune, M. (2007) *J. Biol. Chem.* **282,** 9932–9940
6. Sanes, J. R., and Lichtman, J. W. (2001) *Nat. Rev. Neurosci.* **2,** 791–805
7. Burden, S. J. (1985) *Proc. Natl. Acad. Sci. U.S.A.* **82,** 8270–8273
8. Kim, N., Stiegler, A. L., Cameron, T. O., Hallock, P. T., Gomez, A. M., Huang, J. H., Hubbard, S. R., Dustin, M. L., and Burden, S. J. (2008) *Cell* **135,** 334–342
9. Zhang, B., Luo, S., Wang, Q., Suzuki, T., Xiong, W. C., and Mei, L. (2008) *Neuron* **60,** 285–297
10. Kummer, T. T., Misgeld, T., and Sanes, J. R. (2006) *Curr. Opin. Neurobiol.* **16,** 74–82
11. Lee, Y., Rudell, J., Yechikhov, S., Taylor, R., Swope, S., and Ferns, M. (2008) *Neuroscience* **153,** 997–1007
12. Antolik, C., Catino, D. H., Resneck, W. G., and Bloch, R. J. (2006) *Neuroscience* **141,** 87–100
13. Henriquez, J. P., Webb, A., Bence, M., Bildsoe, H., Sahores, M., Hughes, S. M., and Salinas, P. C. (2008) *Proc. Natl. Acad. Sci. U.S.A.* **105,** 18812–18817
14. Wang, J., Ruan, N. J., Qian, L., Lei, W. L., Chen, F., and Luo, Z. G. (2008) *J. Biol. Chem.* **283,** 21668–21675
15. Fuhrer, C., Gautam, M., Sugiyama, J. E., and Hall, Z. W., (1999) *J. Neurosci.* **19,** 6405–6416
16. Sobel, A., Weber, M., and Changeux, J. P. (1977) *Eur. J. Biochem.* **80,** 215–224
17. Phillips, W. D., Maimone, M. M., and Merlie, J. P. (1991) *J. Cell Biol.* **115,** 1713–1723
18. Ramarao, M. K., and Cohen, J. B. (1998) *Proc. Natl. Acad. Sci. U.S.A.* **95,** 4007–4012
19. Ramarao, M. K., Bianchetta, M. J., Lanken, J., and Cohen, J. B. (2001) *J. Biol. Chem.* **276,** 7475–7483
20. Antolik, C., Catino, D. H., O'Neill, A. M., Resneck, W. G., Ursitti, J. A., and Bloch, R. J. (2007) *Neuroscience* **145,** 56–65
21. Chen, F., Qian, L., Yang, Z. H., Huang, Y., Ngo, S. T., Ruan, N. J., Wang, J., Schneider, C., Noakes, P. G., Ding, Y. Q., Mei, L., and Luo, Z. G. (2007) *Neuron.* **55,** 247–260
22. Zhang, B., Luo, S., Dong, X. P., Zhang, X., Liu, C., Luo, Z., Xiong, W. C., and Mei, L. (2007) *J. Neurosci.* **27,** 3968–3973
23. Dobbins, G. C., Luo, S., Yang, Z., Xiong, W. C., and Mei. L. (2008) *Mol. Brain* **1,** 18
24. Engel, A. G., Ohno, K., and Sine, S. M. (2003) *Nat. Rev. Neurosci.* **4,** 339–352
25. Kusumi, A., Nakada, C., Ritchie, K., Murase, K., Suzuki, K., Murakoshi, H., Kasai, R. S., Kondo, J., and Fujiwara, T. (2005) *Annu. Rev. Biophys. Biomol. Struct.* **34,** 351–378
26. Schreiter, C., Gjoni, M., Hovius, R., Martinez, K. L., Segura, J. M., and Vogel, H. (2005) *ChemBioChem* **6,** 2187–2194
27. Tsien, R. Y. (1998) *Annu. Rev. Biochem.* **67,** 509–544
28. Keppler, A., Pick, H., Arrivoli, C., Vogel, H., and Johnsson, K. (2004) *Proc. Natl. Acad. Sci. U.S.A.* **101,** 9955–9959
29. Guignet, E. G., Segura, J. M., Hovius, R., and Vogel, H. (2007) *ChemPhysChem* **8,** 1221–1227
30. Schütz, G. J., Schindler, H., and Schmidt, T. (1997) *Biophys. J.* **73,** 1073–1080
31. Lommerse, P. H., Snaar-Jagalska, B. E., Spaink, H. P., and Schmidt, T. (2005) *J. Cell Sci.* **118,** 1799–1809
32. Kusumi, A., Sako, Y., and Yamamoto, M. (1993) *Biophys. J.* **65,** 2021–2040
33. Ewers, H., Smith, A. E., Sbalzarini, I. F., Lilie, H., Koumoutsakos, P., and Helenius, A. (2005) *Proc. Natl. Acad. Sci. U.S.A.* **102,** 15110–15115
34. Ferrari, R., Manfroi, A., and Young, W. (2001) *Physica D* **154,** 111–137
35. Saxton, M. J., and Jacobson, K. (1997) *Annu. Rev. Biophys. Biomol. Struct.* **26,** 373–399
36. Ohno, K., Engel, A. G., Shen, X. M., Selcen, D., Brengman, J., Harper, C. M., Tsujino, A., and Milone, M. (2002) *Am. J. Hum. Genet.* **70,** 875–885
37. Müller, J. S., Baumeister, S. K., Schara, U., Cossins, J., Krause, S., von der Hagen, M., Huebner, A., Webster, R., Beeson, D., Lochmüller, H., and Abicht, A. (2006) *Brain* **129,** 2784–2793
38. Kasai, Y., Hashimoto, S., Yamada, T., Sese, J., Sugano, S., Matsushima, K., and Morishita, S. (2005) *Nucleic Acids Res.* **33,** D550–D552
39. Gajsek, N., Jevsek, M., Mars, T., Mis, K., Pirkmajer, S., Brecelj, J., and Grubic, Z. (2008) *Chem. Biol. Interact.* **175,** 50–57
40. Frail, D. E., Musil, L. S., Buonanno, A., and Merlie, J. P. (1989) *Neuron* **2,** 1077–1086
41. Gervásio, O. L., and Phillips, W. D. (2005) *J. Physiol.* **562,** 673–685
42. Barrantes, F. J., Bermudez, V., Borroni, M. V., Antollini, S. S., Pediconi, M. F., Baier, J. C., Bonini, I., Gallegos, C., Roccamo, A. M., Valles, A. S., Ayala, V., and Kamerbeek, C. (2010) *J. Mol. Neurosci.* **40,** 87–90
43. Kellner, R. R., Baier, C. J., Willig, K. I., Hell, S. W., and Barrantes, F. J. (2007) *Neuroscience* **144,** 135–143
44. Stetzkowski-Marden, F., Gaus, K., Recouvreur, M., Cartaud, A., and Cartaud, J. (2006) *J. Lipid Res.* **47,** 2121–2133
45. Allen, J. A., Halverson-Tamboli, R. A., and Rasenick, M. M. (2007) *Nat. Rev. Neurosci.* **8,** 128–140
46. Hezel, M., de Groat, W. C., and Galbiati, F. (2010) *Mol. Biol. Cell* **21,** 302–310
47. Suzuki, K. G., Fujiwara, T. K., Sanematsu, F., Iino, R., Edidin, M., and Kusumi, A. (2007) *J. Cell Biol.* **177,** 717–730
48. Suzuki, K. G., Fujiwara, T. K., Edidin, M., and Kusumi, A. (2007) *J. Cell Biol.* **177,** 731–742
49. Meier, J., Vannier, C., Sergé, A., Triller, A., and Choquet, D. (2001) *Nat. Neurosci.* **4,** 253–260
50. Pato, C., Stetzkowski-Marden, F., Gaus, K., Recouvreur, M., Cartaud, A., and Cartaud, J. (2008) *Chem. Biol. Interact.* **175,** 64–67